Numerical simulation of titanium alloy hip replacement implants behaviour under static and dynamic loads

Tamara Smoljanić[1], Aleksa Milovanović[1], Simon Sedmak[1], Ljubica Milović[2] and Aleksandar Sedmak[3]

[1]Innovation Center of the Faculty of Mechanical Engineering, Belgrade, Serbia
**University of Belgrade, Faculty of Technology and Metallurgy, Belgrade, Serbia*
[3]University of Belgrade, Faculty of Mechanical Engineering, Belgrade, Serbia

Abstract

This paper presents development of numerical models for simulation of the behaviour of titanium alloy hip implants under static and dynamic loads, which is a part of extensive research involving the structural integrity of such implants under various loading conditions, as well as under exposure to aggressive environments. Numerical models were created in ABAQUS and ANSYS software packages, in order to determine the stress/strain distribution, the number of cycles to failure and stress intensity factors, for two different hip implant geometries. The ABAQUS models were used for static and ANSYS models for dynamic loads. The next stage in this analysis involved comparing these two cases, to determine the one with the better behaviour, depending on the exploitation conditions, which can greatly vary between different groups of patients. The targeted patient weight for all numerical simulations was 90 kg, while failure assessment diagrams were made for both implant geometries, assuming a crack length of 1 mm.

Keywords: hip implants; Ti-6Al-4V; Finite element method; Fatigue crack; Failure assessment diagram.

Available on-line at the Journal web address: http://www.ache.org.rs/HI/

ORIGINAL SCIENTIFIC PAPER

UDC: 519.876.5: 616 089. 843:616.728.2:669.295

Hem. Ind. **77(4)** 283-292 (2023)

1. INTRODUCTION

Design of hip implants is of great importance, due to the complex loading and exploitation conditions. The most important factors to consider include the selection of material and the geometry of the implant. Materials should be both resistant to various adverse effects (corrosion and fatigue being the most common problems), while sufficiently safe for use. Previous experience, especially in recent decades, has shown that titanium-based alloys represent a good choice for such implants, due to their suitable mechanical properties, resistance to corrosion, and biocompatibility [1-4]. Geometry plays a significant role as it can directly lead to stress concentrations in certain locations (usually in cases where there are sharp angles or noticeable changes in the cross-section). One of the questions in this research was related to the thickness of the neck part of the implant – would the increase in the thickness be an actual improvement? While having a larger load-bearing cross-section certainly helps in increasing the work life of the implant, it also limits mobility.

For the purpose of the present research, the finite element method was used, both in its classic and extended forms [5-11], in order to determine behaviour of the models with different neck geometries under both static and dynamic loads. These loads were defined in accordance with the most extreme cases which could occur in real conditions, such as stumbling [11]. The extended finite element method was used for fatigue crack growth simulations, since it represents an effective and reliable means of simulating fatigue and was developed for that specific purpose.

Corresponding authors: Tamara Smoljanić, Innovation Center of the Faculty of Mechanical Engineering, Belgrade, Serbia
E-mail: tmijatovic@mas.bg.ac.rs
Paper received: 18 November 2022; Paper accepted: 15 October 2023; Paper published: 1 December 2023.
https://doi.org/10.2298/HEMIND2211180026S

2. MATERIALS AND METHODS

2. 1. Experimental basis

Experimental investigation of the hip implants included tensile tests, fatigue tests and determining of chemical composition of material. The hip implant (an example of which, along with its components, can be seen in Figure 1 was made of titanium-aluminium-vanadium alloy (Ti-6Al-4V), known as Titanium Grade 5 alloy, which was initially used in the aerospace industry, but has also found wide application in biomedicine. It exhibits a favourable combination of mechanical properties, biocompatibility, corrosion, and wear resistance, and in this case, the mechanical properties were the most important since they were used as the input data for the numerical calculations. Namely, yield stress and tensile strength are needed for the modelling, and they were experimentally determined [7] as follows:

- Yield stress – 881 MPa
- Tensile strength – 971 MPa

Additionally, the elasticity module of 120 GPa was adopted, along with a Poisson's ratio of 0.3. To performing the fatigue crack growth analyses in ANSYS, it is necessary to define the Paris law coefficients [12], in accordance with the well known formula (Eq. (1)):

$$\frac{\mathrm{d}a}{\mathrm{d}N} = C\Delta K^{m} \tag{1}$$

Where a is the crack length, N is the number of cycles, ΔK is the stress intensity threshold, and C and m represent the coefficients - C was determined to be 6.72×10^{-13} and m was 2.2. Finally, the fracture toughness of this material was needed in order to draw the failure assessment diagram during the later stage of these simulations. Fracture toughness, in this case, was K_{Ic} = 2100 MPa mm$^{0.5}$ [7].

Figure 1. An example of a real hip implant with its components

The material fatigue crack growth resistance was determined by applying the ASTM E647 standard procedure [12], which prescribes measurement of the fatigue crack growth rate da/dN, where a is the crack length and N is the number of cycles of applied load. Experimental testing of Ti-6Al-4V alloy was described previously [12]. Characteristic diagrams of the fatigue crack growth rate, that the da/dN -change in the range of the fatigue threshold values, ΔK, for the TI-6Al-4V alloy tested at room temperature are shown in [12].

The most commonly used alloy for orthopaedic applications is Ti-6Al-4V, due to its high ratio of strength and weight, good corrosion resistance, and positive biocompatibility. The chemical composition of the alloy used in this paper is given in Table 1., as the average value of a more detailed test [12].

Table 1. Chemical composition of the alloy

Element	Al	V	C	Fe	N	O	H	Ti
Content, %	6.67	4.08	0.012	0.24	0.018	0.08	0.001	remain

The tensile properties were determined by using micro-specimens, as defined by the standard ISO 6892-1:2016 [12]. More detailed results of testing of tensile properties are given in [12].

Fracture toughness is measured by using compact tension (CT) specimens, and a detailed overview of the results can be found in literature [12]. These results indicated relatively brittle behaviour, in accordance with a thickness that has met the plane-strain condition.

As it was shown previously, this particular titanium alloy has a strength value above the titanium average and good resistance to fatigue, allowing it to withstand a considerable number of loading cycles [12], as will be shown by the results of the numerical simulations presented.

2. 2. Previous numerical simulations using static loads

This section of the paper presents the initial numerical calculations, which were performed with static loading, for the purpose of determining the critical locations in the hip implant, where cracks would be expected to occur. Its goal was to accurately locate the area in the model, which is subjected to highest tensile stresses, and was expected in the implant neck area.

The finite element method, used in order to simulate the behaviour of titanium alloy hip im-plants under different loading conditions, was done in ABAQUS v6.14 (Dassault Systèmes Simulia Corp., Providence, RI, USA) for the former and ANSYS R19.2 (ANSYS, Inc., Canonsburg, PA, USA) for the latter case. This decision was made after some practical experience had shown that the ANSYS software is somewhat easier and faster to use for fatigue-related calculations.

Two versions of the hip implants were considered in these simulations – one with a neck diameter of 9 mm and the other with 14.6 mm. The load was defined based on a weight of 90 kg [7], in the form of a concentrated force. For this calculation the worst-case scenario was assumed, which involved stumbling, thus greatly increasing the intensity of the load. Boundary conditions were defined as fixed along the surface of the stem.

Some of the results of static simulations, performed in the previous analyses in order to determine the locations where highest tensile stresses would occur, can be seen in Figure 2 [8].

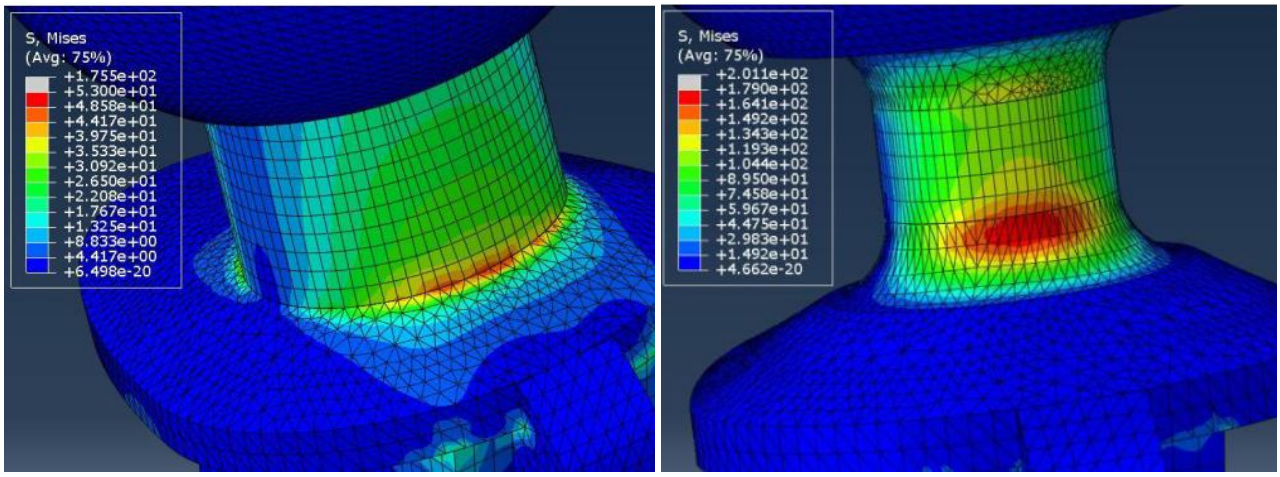

Figure 2. Left- Stress distribution for the model with a 14.6 mm neck; Right- Stress distribution for the model with a 9 mm neck [8]. Permissions under Attribution 4.0 International (CC BY-NC-ND 4.0 DEED)

These results have shown that the decrease in neck thickness affects considerably the stress magnitudes, causing maximum tensile stresses to increase more than three times – in the case of the 14.6 mm neck, their value was around 52 MPa, whereas, for the 9 mm neck, they were 179 MPa. As expected, stress concentrations were most prominent in the transition area between the neck and the collar (Figure 3). This finding was important since it provided the exact location where a fatigue crack would be most likely to initiate. This assumption was used as the base for the extended finite element method (XFEM) simulations which included the fatigue crack growth.

As for the fatigue crack growth simulations, the model that was used can be seen in Figure 3 for both investigated implant geometries. Boundary conditions were defined in the same way as for the static models (stem-bone contact was fixed), and the load was also applied as a concentrated force, with a magnitude that corresponded to a 90 kg person during normal walk (the loading here is cyclic, since simulation of repeated stumbling would not be reasonable).

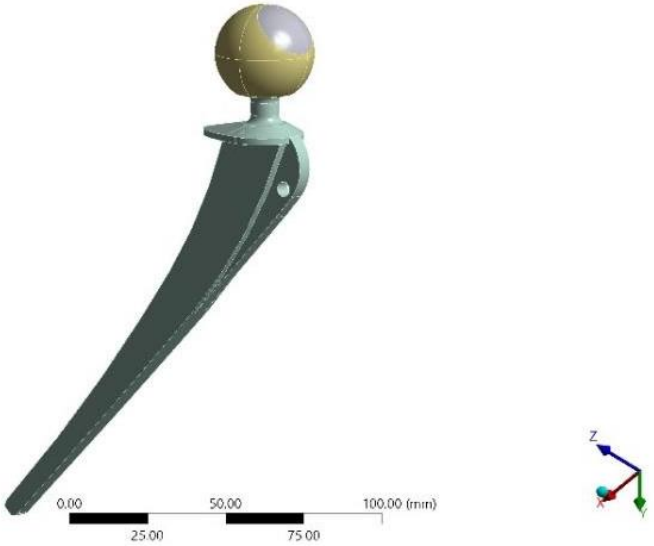

Figure 3. Geometry of the finite element model used for fatigue crack growth simulations in ANSYS [7]. Permissions under Attribution 4.0 International (CC BY 4.0)

The initial crack length was adopted as 1 mm since this is considered to be the minimum crack length that can be detected by using non-destructive test methods. The crack was placed at the stem-collar connection area, where the highest tensile stresses were determined during the static loading simulation stage. It should be noted that there was a noticeable difference in finite element meshes for the static and dynamic models – for static ones, a combination of linear hexahedral (HEX) and tetrahedral (TET) elements were used, whereas dynamic load models were made entirely out of TET elements, due to the specifications of the ANSYS software, i.e., the fatigue crack growth can only be simulated in a TET mesh.

3. RESULTS OF NEW FATIGUE BEHAVIOUR SIMULATIONS

Results of fatigue crack growth simulations are shown in the following section of the paper, starting with the stress distribution around the fatigue crack during its growth, shown in Figures 4 and 5.

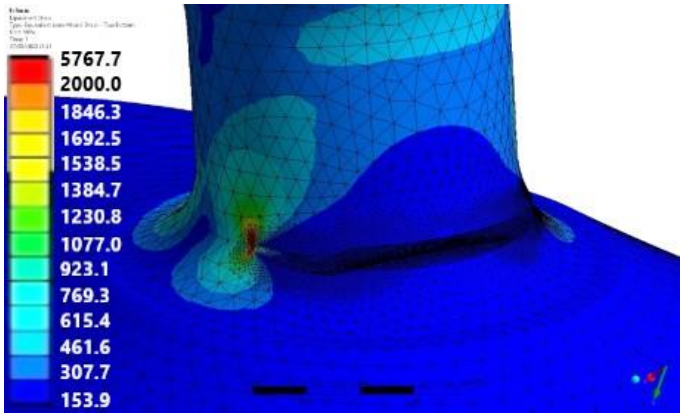

Figure 4. Fatigue crack growth in the 9 mm neck model [7]. Permissions under Attribution 4.0 International (CC BY 4.0)

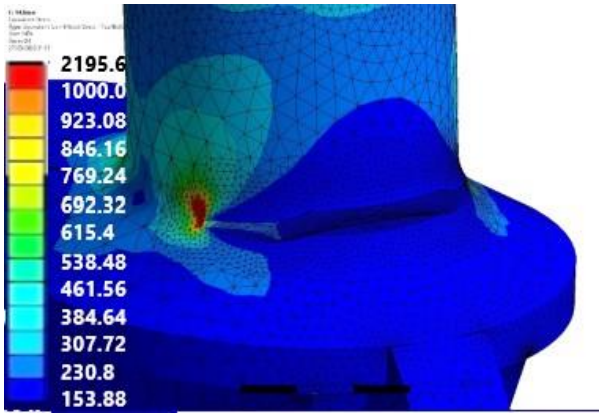

Figure 5. Fatigue crack growth in the 14.6 mm neck model [7]. Permissions under Attribution 4.0 International (CC BY 4.0)

As expected, the highest stresses were concentrated around the crack tip, and their values in the case of the 9 mm neck were almost three times larger compared to the 14.6 mm case (5760 and 2195 MPa, respectively). High values of stress were the result of using the linear-elastic fracture mechanics' approach. Since elastic-plastic fracture mechanics cannot be still reliably combined with XFEM fatigue simulations, linear-elastic fracture mechanics (LEFM) was adopted. The relation between the obtained numbers of cycles for both cases was also similar – around three times greater for the 14.6 mm neck

(5.2 million *vs.* 1.6 million). The aforementioned results indicated that the model with a wider neck has a considerably longer fatigue life. Its design allowed the fatigue crack to propagate to a much greater length compared to the 9 mm model. Of course, there is still a disadvantage to the 14.6 mm model, mainly in terms of mobility. Thus, additional analyses were performed to further determine the effects of geometry on hip implant integrity in more detail.

For this purpose, stress intensity factors were calculated for both models. Results were taken for crack lengths of approximately 1 mm (initial crack length) and are shown in Figure 6.

Following this step, it was concluded that the results would be more representative if an additional model was included, whose neck thickness would be between the other two values. This neck thickness was adopted as the mean value of 9 and 14.6 mm, *i.e.* 11.8 mm. Stress intensity factor results for this model are shown in Figure 7. This was done in order to determine the transition between different dimensions in a more detailed manner, and because creating an additional model was simple with the existing base, since the only change was the neck thickness.

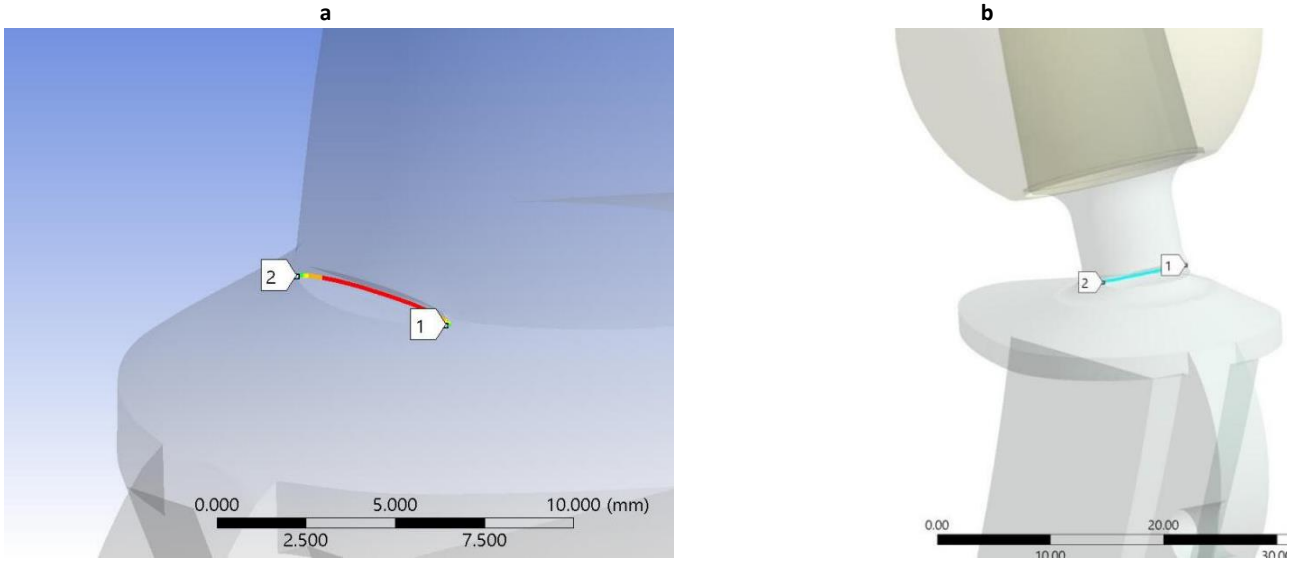

Figure 6. Stress intensity factors for the 14.6 mm neck model (a) and 9 mm neck model (b)

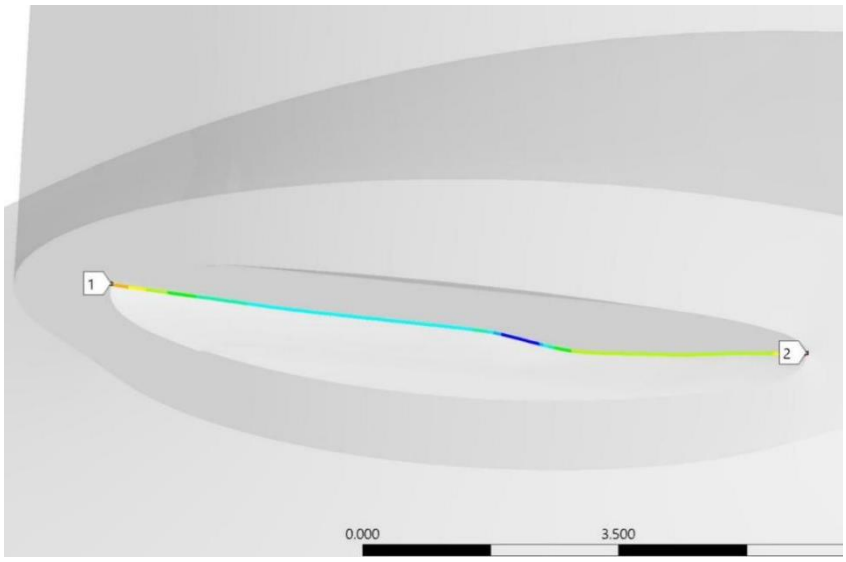

Figure 7. Stress intensity factors (SIFs) for 11.8 mm neck model

The reason for determining stress intensity factors (SIFs) was to create Failure assessment diagrams for both models and observe the potential differences between them. Analysis of the Failure assessment diagrams for these models will be shown in the following section of the paper.

4. FAILURE ASSESSMENT DIAGRAMS FOR HIP IMPLANTS

Failure assessment diagrams (FAD) represent a relatively simple and very reliable methodology for assessing the integrity of structures [13-19]. They are based on stresses and stress intensity factors for a given structure and indicate the probability of failure, as well as its nature (brittle fracture or plastic collapse). The basic concept is to establish the so-called limit curve in the coordinate system of two non-dimensional quantities, $S_r=\sigma/\sigma_c$ and $K_r=K_I/K_{Ic}$, as follows. S_r is the ratio of stresses in the observed material (σ) and its yield stress (σ_c), and K_r is the ratio of stress intensity factors around the crack (K_I) and the material's fracture toughness (K_{Ic}) (critical value of SIF). The starting point is to apply the Dugdale model valid for plane stress state and ideal plasticity, *i.e.* to equalize the stress intensity factors for a crack length (a)+plastic zone size (ρ) and for a closure forces, taken as yield stress in a plastic zone, Figure 8.

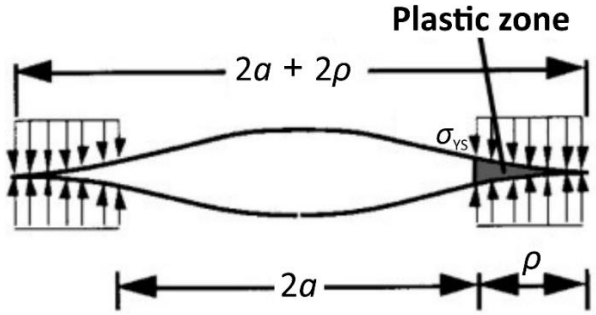

Figure 8 Dugdale model, where σ_{YS} represents yield stress

In this way, the following relation between the stress, crack length a and the plastic zone size ρ, is obtained (Eq. (2)):

$$\sigma\sqrt{\pi(a+\rho)}=\frac{2\sigma_{YS}}{\sqrt{\pi}}\sqrt{a+\rho}\arccos\left(\frac{a}{a+\rho}\right)\Rightarrow\left(\frac{a}{a+\rho}\right)=\cos\left(\frac{\pi\sigma}{2\sigma_{YS}}\right) \tag{2}$$

By using an expression for displacement v (3), one can get now the crack tip opening displacement (*Crack Tip Opening Displacement - CTOD*), denoted by δ:

$$\delta=\frac{8}{\pi}\frac{\sigma_{YS}a}{E}\ln\left|\sec\left(\frac{\pi\sigma}{2\sigma_{YS}}\right)\right| \tag{3}$$

Based on this expression and relation for the effective stress intensity factor, we have (Eq. (4)):

$$K_{eff}=\sqrt{\sigma_{YS}\delta} \tag{4}$$

valid for plane stress and ideal plasticity, one gets (Eq. (5)):

$$K_{eff}=\sigma_{YS}\sqrt{\pi a}\left[\frac{8}{\pi^2}\ln\sec\frac{\pi}{2}\frac{\sigma}{\sigma_{YS}}\right]^{1/2} \tag{5}$$

The next step in this procedure is to replace yield stress σ_{YS} with a more realistic quantity, the collapse (critical) stress, σ_C, which depends not only on the material, but also on geometry. For a structure under tension, plastic collapse occurs when the 'net' stress in cross section containing a crack reaches the critical value, σ_C. Finally, one can get the limit curve where the effective stress intensity factor is given in non-dimensional form (Equation (6)), K_{eff}/K_I:

$$\frac{K_{eff}}{K_I}=\frac{\sigma_c}{\sigma}\left[\frac{8}{\pi^2}\ln\sec\frac{\pi}{2}\frac{\sigma}{\sigma_c}\right]^{1/2} \tag{6}$$

where $K_I=\sigma\sqrt{\pi a}$. If K_{eff} is replaced by K_{Ic} and the following non-dimensional forms, $S_r=\sigma/\sigma_c$ and $K_r=K_I/K_{Ic}$, are used, one gets the final form (Eq- (7)) of the limit curve:

$$K_r=S_r\left[\frac{8}{\pi^2}\ln\sec\left(\frac{\pi}{2}S_r\right)\right]^{-1/2} \tag{7}$$

The limit curve separates the safe and potentially unsafe regions in the FAD, as shown in Figure 9, where points for all three hip implants are presented, calculated as explained in the following text.

To determine the points for the FAD for all hip implants, it was necessary to determine relevant stresses and stress intensity factors and then calculate their ratios – between the actual stresses and the yield stress and between the SIFs and fracture toughness, K_{Ic}. Values of the yield stress and K_{Ic} were determined as explained in the earlier part of the paper and were used as referent values in the calculation.

As for the stress in the model, the adopted values were taken from the model, based on the corresponding SIF results, in other words, stresses at the crack length of 1 mm, since that was the length for which stress intensity factors were determined. In the case of the 9 mm neck model, with the corresponding SIF value of 1441 MPa$\sqrt{}$mm, stress was 726 MPa, whereas for the 14.6 mm neck model the SIF and stress values were 348 MPa mm$^{0.5}$ and 175 MPa, respectively. Finally, for the third, "middle" model, the SIF value was 891 MPa mm$^{0.5}$, and the corresponding stress was 449 MPa.

By using the previously known values of yield stress for Ti-6Al-4V (881 MPa) and its fracture toughness (2100 MPa mm$^{0.5}$), the following coordinates were obtained for all three models in the FAD:

- For the 14.6 mm neck model – S_r = 0.2, K_r = 0.16
- For the 11.8 mm neck model – S_r = 0.51, K_r = 0.42
- For the 9 mm neck model – S_r = 0.82, K_r = 0.69

These points are shown in the FAD (Fig. 9). As can be seen, all three points fall in the safe region of the diagram (below the curve). As expected, the 9 mm model result is the least favourable and is quite near to the safe/failure regions limit curve. Considering that the final fatigue crack length obtained by the simulations given in [12] for the 9 mm model was much shorter than the one in 14.6 mm model (3.45 *vs.* 150 mm), the position of the point corresponding to the 9 mm model makes sense, taking into account the assumed initial crack length of 1 mm used for the SIF calculations.

Of course, the 14.6 mm neck version has the best values of S_r and K_r, making it the safest of the three models, with its corresponding point being close to the FAD origin. The model with an 11.8 mm neck was halfway between the two, also being much safer than the 9 mm one.

Since the point corresponding to the 9 mm neck was the most critical, *i.e.* closest to the limit curve, it was of particular interest to estimate the approximate crack length at which the point would coincide with the curve. Based on the interpolation of this point, it was determined that the limit curve stress intensity factor ratio (y-axis) would be around 1680 MPa mm$^{0.5}$. Based on this, it was determined that the corresponding crack length would be around 4 mm.

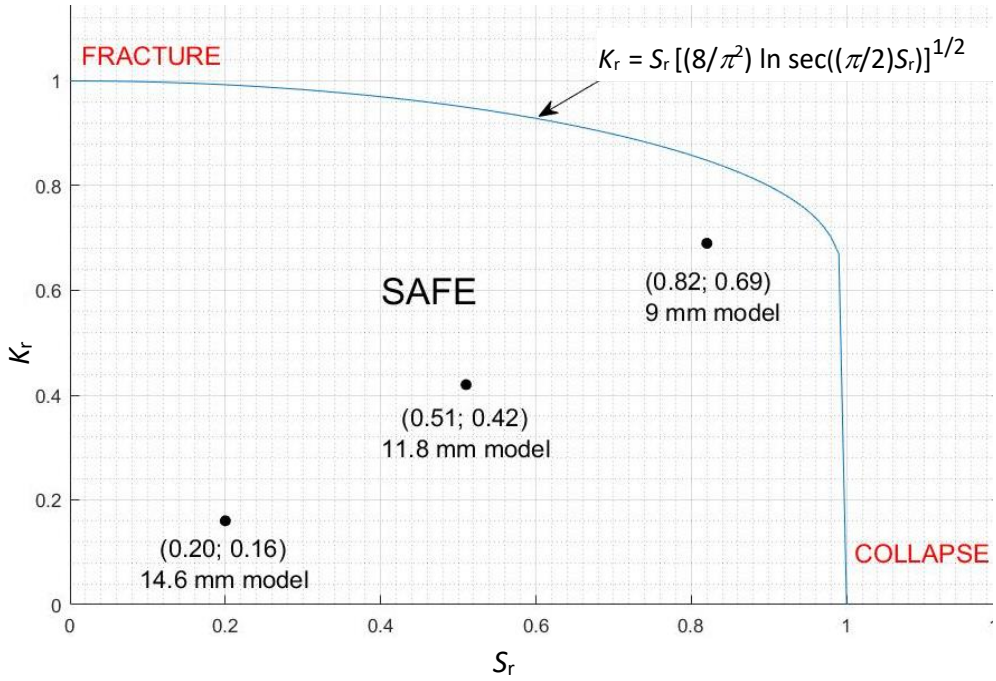

Figure 9. Failure assessment diagram for three different hip joint models

5. DISCUSSION

Results obtained for all three models also provided additional insights into the structural integrity of hip implants in the presence of a 1 mm fatigue crack, particularly in terms of how they are expected to fail – the thinnest neck being the closest to the limit curve. Based on the obtained fatigue crack lengths at failure in the previous simulations, and the somewhat high SIFs in this case, it was assumed that the 9 mm neck hip implant would have a predominantly brittle fracture. However, according to the FAD, it has exceeded its expectations and was closer to plastic collapse. Based on the diagram, the other two cases would eventually show similar behaviour, at higher stress/SIF levels. Anyhow, one should keep in mind that the FAD presented here is level I, based on the simple plasticity model, whereas levels 2 and 3 would provide additional plasticity reserve and less conservative, but still reliable failure assessment [21].

It needs to be emphasized that results for different crack lengths and/or geometries will not always necessarily align like in Figure 9. In the present case, the SIF value was almost equal to the mean value of the other two, but that was most likely a coincidence, and it does not suggest that adopting dimensions that are the average of two values will always result in SIFs and stresses which will also represent mean values of the initial two dimensions.

Both static and dynamic analyses confirmed that the 14.6 mm model has the best performance in terms of structural integrity (resistance to fatigue crack growth in this case). In fact, it has considerably better performance, with a notable difference in the number of cycles, and a significantly lower probability of failure, as determined by numerical simulations and the FAD. This suggests that hip implants with such geometry would be most favourable in cases where there is no need for increased hip mobility since it would be constrained by the aforementioned thick neck. In such cases, the patients would be able to use a single hip implant for extended periods of time without the need for replacement. Also, if a fatigue crack was to initiate in the implant, there would be a significantly wider time interval during which this problem could be detected, compared to the 9 mm case, where the fatigue crack would propagate to its maximum length considerably faster. The hip implant with the 11.8 mm neck should be also kept in mind, as it would offer the best compromise between mobility and fatigue life, while staying sufficiently safe.

Thus, the goal of this research, involving the analysis of fatigue behaviour of hip implants made of Ti-6Al-4V, was achieved in several ways, *i.e.* numerical and analytical - providing an accurate base of results. It also demonstrated the efficiency and effectiveness of numerical simulations, even when using different software.

5. CONCLUSIONS

In this paper three hip replacement implant geometries were considered (one of which was only analysed numerically), differing in thickness of the neck area. The neck area of the implant is essential for load distribution during physical activities, *i.e.* walking, running, climbing stairs, *etc*. Both geometries have specific advantages, *i.e.* thicker geometry provides longer structural life of the component, and thinner one increases patient mobility.

In order to estimate such claims, static and dynamic analyses were conducted: static for estimating locations with the highest stress concentrations and based on the obtained results research dynamic tests were conducted with initiated defects (*i.e.* cracks) on such locations. This paper is a continuation of previous research activities, including FAD for both geometries and one intermediate case, to get a better insight into selected hip implant structural integrity. All of the obtained points in FAD fall within the safe region, with thicker geometries being safer (*i.e.* closer to the FAD origin).

Acknowledgement: *The authors would like to thank the support from the Ministry of Education, Science and Technological Development of the Republic of Serbia by Contract Nos. 451-03-68/2022-14/200105 and 451-03-68/2022-14/200135.*

REFERENCES

[1] Sarraf M, Ghomi ER, Alipour S, Ramakrishna S, Sukiman NL. A state-of-the-art review of the fabrication and characteristics of titanium and its alloys for biomedical applications. *Bio-des. Manuf.* 2022; 5: 371-395. https://doi.org/10.1007/s42242-021-00170-3.

[2] Kirmanidou Y, Sidira M, Drosou ME, Bennani V, Bakopoulou A, Tsouknidas A, Michailidis N, Michalakis K. New Ti-Alloys and Surface Modifications to Improve the Mechanical Properties and the Biological Response to Orthopedic and Dental Implants: A Review. *BioMed Res Inter.* 2016; 2908570. https://doi.org/10.1155/2016/2908570.

[3] Eisenbarth E, Velten D, Muller M, Thull R, Breme J. Biocompatibility of beta-stabilizing elements of titanium alloys. *Biomaterials* 2004; 25(26): 5705-5713. https://doi.org/ 10.1016/j.biomaterials.2004.01.021.

[4] Niinomi M, Nakai M, Hieda J. Development of new metallic alloys for biomedical applications. *Acta Biomater.* 2012; 8(11): 3888-3903. https://doi.org/ 10.1016/j.actbio.2012.06.037.

[5] Sedmak A, Čolić K, Burzić Z, Tadić S. Structural integrity assessment of hip implant made of cobalt-chromium multiphase alloy. *Struct Integr Life.* 2010; 10(2): 161-164. http://divk.inovacionicentar.rs/ivk/ivk10/161-IVK2-2010-AS-KC-ZB-ST.pdf.

[6] Milovanović A, Sedmak A, Čolić K, Tatić U, Đorđević B. Numerical analysis of stress distribution in total hip replacement implant. *Struct Integr Life.* 2017; 17(2): 139-144. http://divk.inovacionicentar.rs/ivk/ivk17/139-IVK2-2017-AM-AS-KC-UT-BDj.pdf.

[7] Milovanović A, Sedmak A, Grbović A, Mijatović T, Čolić K. Design Aspects of Hip Implant Made of Ti-6Al-4V Extra Low Interstitials Alloy. *Procedia Struct Integr.* 2020; 26: 299-305. https://doi.org/10.1016/j.prostr.2020.06.038.

[8] Mijatović T, Milovanović A, Sedmak A, Milović Lj, Čolić K. Integrity assessment of reverse engineered TI-6AL-4V ELI total hip replacement implant. *Struct Integr Life.* 2019; 19(3): 237-242. http://divk.inovacionicentar.rs/ivk/ivk19/237-IVK3-2019-TM-AM-AS-LjM-KC.pdf.

[9] Sedmak A, Čolić K. Fracture and fatigue behaviour of implants made of Ti alloys. *Procedia Struct Integr.* 2019; 23: 45-50. https://doi.org/10.1016/j.prostr.2020.01.061.

[10] Čolić K, Sedmak A, Legweel K, Milošević M, Mitrović N, Mišković Ž, Hloch S. Experimental and numerical research of mechanical behaviour of titanium alloy hip implant. *Teh Vjesn.* 2017; 24(3): 709-713. https://doi.org/10.17559/TV-20160219132016.

[11] Čolić K, Sedmak A, Grbović A, Tatić U, Sedmak SA, Đorđević B. Finite element modeling of hip implant static loading. *Procedia Eng.* 2016; 149: 257-262. https://doi.org/10.1016/j.proeng.2016.06.664.

[12] Sedmak A, Čolić K, Grbović A, Balać I, Burzić M. Numerical analysis of fatigue crack growth of hip implant. *Eng Fract Mech.* 2019; 216: 106492. https://doi.org/ 10.1016/j.engfracmech.2019.106492.

[13] Sedmak A, Kirin S, Martić I, Jeremić L, Vučetić I, Golubović Sedmak T, Sedmak SA. Structural Integrity and Life Assessment of Pressure Vessels - Risk Based Approach. In: *Experimental and Computational Investigations in Engineering, Proceedings of the International Conference of Experimental and Numerical Investigations and New Technologies*, *CNNTech2020*, Springer, 2020: 274–293. https://doi.org/10.1007/978-3-030-58362-0_16.

[14] Golubović T, Sedmak A, Spasojević Brkić V, Kirin S, Rakonjac I. (2018). Novel Risk Based Assessment of Pressure Vessels Integrity. *Teh Vjesn.* 2018; 25(3): 803-807. https://doi.org/ 10.17559/tv-20170829144636.

[15] Kirin S, Jeremić L, Sedmak A, Martić I, Sedmak SA, Vučetić I, Golubović T. Risk based analysis of RHPP penstock structural integrity. *Frat ed Integrita Strutt.*2020; 14(53): 345-352. https://doi.org/ 10.3221/IGF-ESIS.53.27.

[16] Golubović T, Sedmak A, Spasojević Brkić V, Kirin S, Veg, E. Welded joints as critical regions in pressure vessels – Case study of vinyl-chloride monomer storage tank. *Hem Ind.* 2018; 72(4): 177-182. https://doi.org/10.2298/HEMIND171009006G.

[17] Sedmak A, Zaidi R, Vujičić B, Šarkočević Ž, Kirin S, Stamenić Z, Đukić M, Bakić G. Corrosion effects on structural integrity and life of oil rig drill pipes. *Hem Ind.* 2022; 76(3):167-177. https://doi.org/10.2298/HEMIND220222014S.ž

[18] Zaidi R, Sedmak A, Kirin S, Grbović A, Wei L, Lazić Vulićević Lj, Šarkočević Ž. Risk assessment of oil drilling rig welded pipe based on structural integrity and life estimation. *Eng Fail Anal.* 2020; 112: 104508. https://doi.org/10.1016/j.engfailanal.2020.104508.

[19] Kirin S, Sedmak A, Zaidi R, Grbović A, Šarkočević Ž. Comparison of experimental, numerical and analytical risk assessment of oil drilling rig welded pipe based on fracture mechanics parameters. *Eng Fail Anal.* 2020; 114: 104600. https://doi.org/10.1016/j.engfailanal.2020.104600

[20] Chen, X.G, Wu, X.G, Yan, M.G. Dugdale model for strain hardening materials. *Eng. Fract. Mech.* 1992; 41(6):843-871. https://doi.org/10.1016/0013-7944(92)90236-8.

[21] Lee, J-S, Ju, J-B, Jang, J-I, Kim, W-S, Kwon, D. Weld crack assessments in API X65 pipeline: failure assessment diagrams with variations in representative mechanical properties. *Mater Sci Eng. A* 2004; 373:122-130. https://doi.org/10.1016/j.msea.2003.12.039.

Numerička simulacija implantata kuka od legure titanijuma pod statičkim i dinamičkim opterećenjima

Tamara Smoljanić[1], Aleksa Milovanović[1], Simon Sedmak[1], Ljubica Milović[2] and Aleksandar Sedmak[3]

[1]*Inovacioni Centar Mašinskog fakulteta, Beograd, Srbija*
[2]*Univerzitet u Beogradu, Tehnološko-Metalurški fakultet, Beograd, Srbija*
[3]*Univerzitet u Beogradu, Mašinski fakultet, Beograd, Srbija*

(Naučni rad)

Izvod

U ovom radu je prikazan razvoj numeričkih modela za simulaciju implantata za zamenu zgloba kuka pod statičkim i dinamičkim opterećenjima, kao deo širokog istraživanja koje uključuje procenu integriteta implantata kuka u različitim uslovima, kao što su zamor i korozija. Numerički modeli su napravljeni u ABAQUS i ANSYS softverskim paketima, u cilju procene distribucije napon/deformacija i broja ciklusa do loma, kao i vrednosti faktora intenziteta napona za dve različite geometrije implanta kuka. ABAQUS modeli su korišćeni za simulaciju pod statičkim, a ANSYS modeli za simulaciju pod dinamičkim opterećenjima. Sledeća etapa analize uključuje poređenje ova dva slučaja, kako bi se odredilo koja od ove dve geometrije pruža bolje ponašanje u eksploatacionim uslovima, a koje mogu značajno varirati zavisno od pacijenta. Simulacije su vršene za pacijenta mase 90 kg. Za ovu svrhu, dijagrami procene rizika su napravljeni za obe navedene geometrije, pod pretpostavkom da je dužina inicijalne prsline 1 mm.

Ključne reči: Implantat kuka; Ti-6Al-4V; metoda konačnih elemenata; zamorna prslina; dijagram procene rizika